ORIGINAL ARTICLE

lajss.org Latin American Journal of Solids and Structures

www.lajss.org

A prediction method for the crashworthiness of multi-cell tubes based on machine learning

Hongbin Tang[a,b], Ledan Liu[a,b], Zheng Dou[c], Zihang Li[c]*

[a] National key Laboratory of Advanced Vehicle Integration and Control, Changchun, China. Email: tanghongbin@faw.com.cn
[b] FAW Global R&D Center, Changchun, China.
[c] Jilin University, Changchun, China. Email: douzheng99@foxmail.com, lzx24@mails.jlu.edu.cn

* Corresponding author

https://doi.org/10.1590/1679-7825/e8660

Abstract

This study presents a machine learning framework to predict the crashworthiness of multi-cell tubes. Five distinct cross-sectional designs are selected, and various structural configurations are generated by sampling predefined parameters. The training dataset is generated through finite element (FE) simulations. Using the autoencoder, structural features of the voxelized FE simulations are encoded into a one-dimensional latent space. When combined with thickness information, this latent representation provides a comprehensive description of the tube structure. The prediction model in this study is built using a MLP neural network, selected after a comparative analysis of multiple algorithms. The MLP demonstrates strong predictive capability, achieving errors of 14.21% for mean crushing force and 14.49% for peak crushing force. The method based on an autoencoder and MLP enables rapid and accurate prediction of the crashworthiness of multi-cell tubes. Compared to traditional finite element simulations, which require approximately 2.5 hours to evaluate a single sample, the MLP reduces the prediction time to just 0.079 seconds, significantly lowering computational costs and greatly accelerating the structural optimization process.

Keywords

Multi-cell tubes, Machine learning, Crashworthiness, Autoencoder

Graphical Abstract

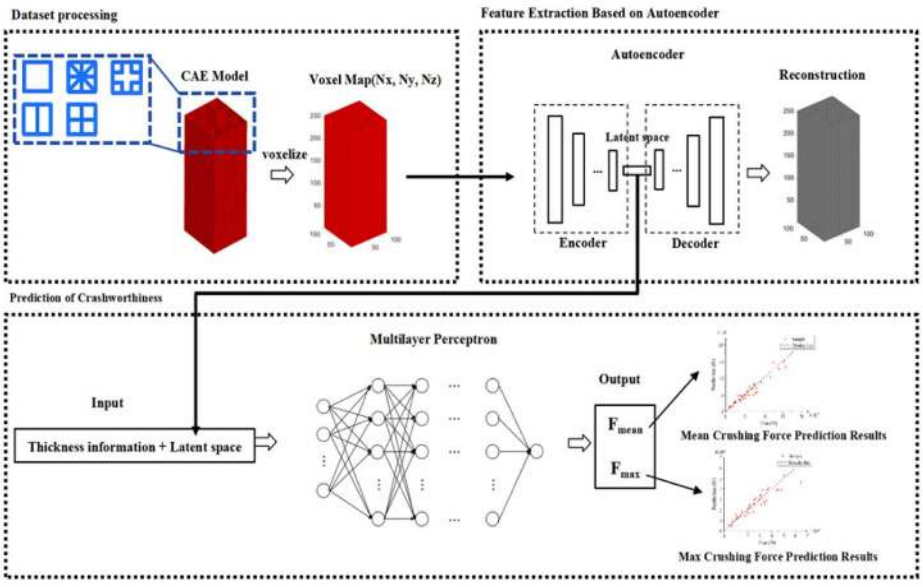

Received april 09, 2025. In revised form june 03, 2025. Accepted june 22, 2025. Available online june 25, 2025.
https://doi.org/10.1590/1679-7825/e8660

Latin American Journal of Solids and Structures. ISSN 1679-7825. Copyright © 2025. This is an Open Access article distributed under the terms of the Creative Commons Attribution License, which permits unrestricted use, distribution, and reproduction in any medium, provided the original work is properly cited.

1. INTRODUCTION

In structural engineering, thin-walled tubes are widely used structural components in aerospace, automotive, architectural, and protective applications. Crashworthiness is a critical design criterion directly influencing the impact resistance and durability of engineering structures[1][2]. In the design process of thin-walled tubes, crashworthiness is always a key factor to be considered.

In recent years, with the rapid development of manufacturing technology[3][4] and materials, various novel multi-cell tubes with complex cross-sections, as shown in Figure 1, have been developed, enhancing their structural performance. The study by Yao and Pang et al.[5] indicates that, within a certain range, as the number of cells in multi-cell tubes increases in axial crushing experiments, the specific energy absorption and load efficiency of the thin-walled tube increase significantly.

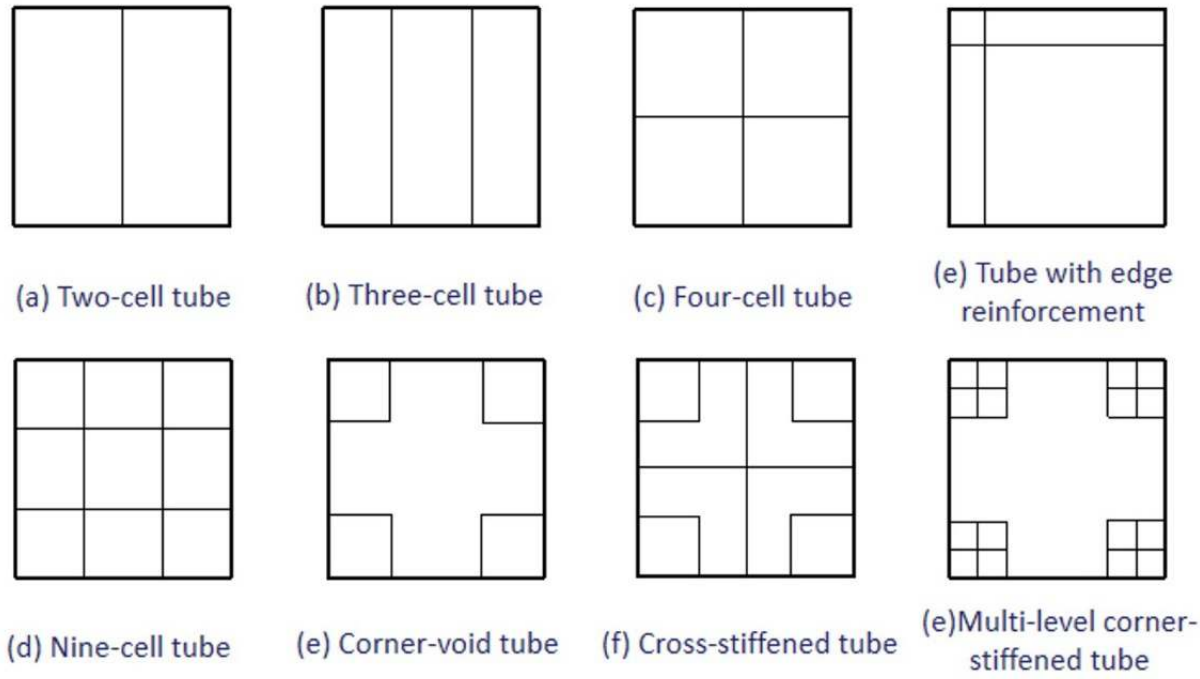

Figure 1. Different structures of multi-cell tubes.

Currently, research on thin-walled tube design is primarily conducted using traditional methods, which are based on theoretical derivations to develop a series of formulas. Zheng and Pang et al.[6] theoretically derived the crashworthiness of transversely variable-thickness multi-cell tubes. Lu et al.[7][8] carried out theoretical derivations for CFRP/Al hybrid multi-cell tubes under axial compression conditions. While theoretical derivations improve the understanding of thin-walled tube behavior, the process is complex, and discrepancies exist between analytical and experimental results.

In recent years, machine learning, as a powerful data-driven approach, has shown great potential in the field of engineering structural design. Jeon J and Kim J et al.[9] estimated the stiffness matrix of thin-walled tube node structures using deep learning methods. Ghasemi M and Silani M et al.[10] predicted the energy absorption of thin-walled tubes through machine learning techniques. Predicting the crashworthiness of thin-walled tubes using machine learning not only enhances accuracy but also effectively addresses the challenges faced by traditional methods. By utilizing large amounts of sample data and integrating machine learning, highly accurate predictions of the energy absorption behavior of thin-walled tubes can be achieved.

This study aims to develop a machine learning model for predicting the crashworthiness of multi-cell tubes. We propose a novel prediction framework that utilizes an autoencoder to extract features from tubes structures[11] and employs a predictive model to estimate crashworthiness based on the extracted features. By leveraging a large amount of sample data and machine learning algorithms, we develop a model capable of highly accurate crashworthiness prediction for thin-walled tubes with strong generalization capabilities, enabling adaptation to different structures and thicknesses. The findings of this study will aid in optimizing the design process, improving crashworthiness, and enhancing structural safety and reliability.

2. CRASHWORTHINESS OF MULTI-CELL TUBES

During the axial crushing process, due to corner reinforcements in rectangular thin-walled tubes, these regions often undergo more severe plastic deformation. This severe plastic deformation introduces significant nonlinearity into the stress-strain relationship, while pronounced geometric alterations further affect energy absorption performance, complicating the interpretation of experimental findings.

Chen and Wierzbicki et al.[12] demonstrated that as the number of cells increases, the deformation bands within the thin-walled tube also increase, introducing greater nonlinearity into the specific energy absorption behavior. Zhang et al.[13] further highlighted that during the axial crushing of multi-cell tubes, the interaction between different cells in terms of force and deformation causes significant differences in their geometric deformation, as shown in Figure 2. This makes the overall deformation pattern more difficult to predict. Additionally, as the deformation process evolves, the distribution of energy absorption becomes more uneven, thereby increasing the difficulty of evaluating its crashworthiness.

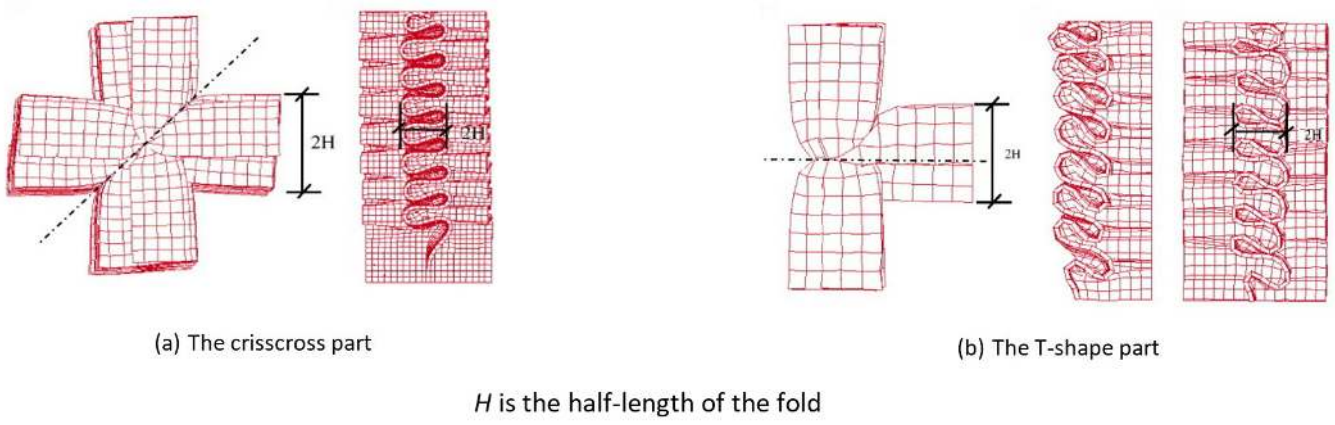

Figure 2. Deformation of multi-cell tubes with different structures[13].

To ensure that multi-cell tubes satisfy crashworthiness criteria under impact conditions, FE models are commonly used to simulate their axial crushing behavior. However, when optimizing these complex structures, repeated simulations with high-fidelity mesh discretization are required to accurately capture detailed deformation mechanisms. This leads to substantial computational and labor costs, making the overall design and optimization process time-consuming and resource-intensive[14]. To address this issue, this study proposes leveraging deep learning models for rapid prediction the peak force and mean crushing force of multi-cell tubes to assisting CAE simulations. This approach significantly shortens the optimization cycle of multi-cell tube design, enabling efficient crashworthiness evaluation and accelerating the structural optimization process.

3. ESTABLISHMENT OF THE MULTI-CELL TUBES MODEL AND STRUCTURAL CHARACTERIZATION

3.1 FE Model of Multi-Cell Tubes

To develop a model for predicting the crashworthiness of multi-cell tubes, this study employs FE simulations to obtain response data and construct a dataset. Compared to experimental data, FE simulation offers advantages such as shorter computational time, lower cost[15].

The goal is to predict the mean crushing force and peak crushing force for multi-cell tubes with various cross-sectional shapes. To generate the sample set required for training the predictive model, this study parameterizes the thin-walled tube structures and employs a Design of Experiments (DOE) approach to create a diverse set of FE models. Figure 3 illustrates the five selected cross-sectional types of thin-walled tubes, which were inspired by the multi-cell tube structures presented in the work of Yao and Pang et al[5]. Among them, five typical and representative configurations were chosen, including the single-cell tube, two-cell tube, three-cell tube, four-cell tube, and corner-void tube. The tube high is fixed at 250 mm, meaning the structure can be represented using three variables: length L, width W, and thickness T.

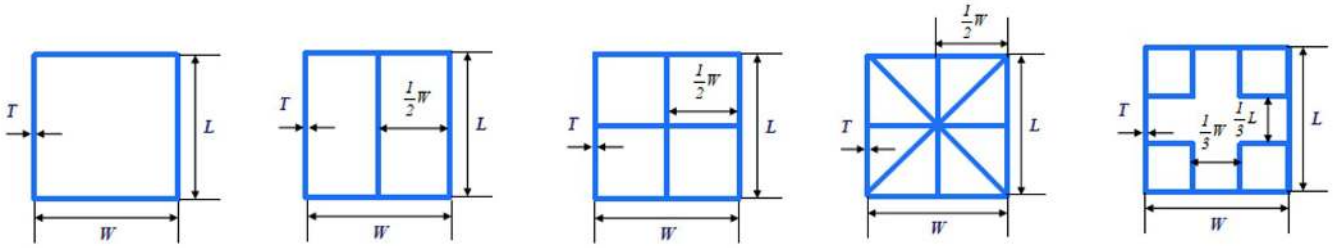

Figure 3. Schematic of Thin-Walled tube Cross-Sections.

Table1.summarizes the variable specifications. The sample data is generated using the Hammersley sampling criterion, which is a quasi-Monte Carlo sampling method[16]. This technique utilizes a pseudorandom number generator to distribute sampling points evenly across the design space following a specific sampling principle. The Hammersley points for an *n*-dimensional sampling space can be determined by the following equation:

$$\left(\frac{z}{N},\Phi_{p1}(z),\Phi_{p2}(z),\cdots,\Phi_{p(n-1)}(z)\right),z=0,1,2,\cdots,N-1 \tag{1}$$

where *N* represents the number of sampling points, and *z* is a non-negative integer represented by a polynomial function, defining an arbitrary sequence as a function of *z*. The Hammersley sampling method ensures better uniformity. In comparison with conventional sampling strategies, it achieves a quadratic-level reduction in the number of required samples. This significant advantage enables its effective application in cases where the response surface is highly nonlinear[17]. In this study, 50 representative samples are randomly selected from the full Hammersley set, ensuring uniform coverage of the design space while reducing computational cost. Part of the experimental design data is shown in Table1..

It is important to emphasize that the geometric parameters in this study are used solely to generate FE models of varying dimensions; they do not serve as inputs to the predictive model. Instead, these parameters and the sampling method are used exclusively for dataset generation.

Table1. Design Variables for Cross-Sectional Parameters.

Variable Type	Length / *L* (mm)	Width / *W* (mm)	Thickness / *T* (mm)
Value Range	[40, 140]	[40, 140]	[1, 2.6]

The axial crushing simulation of thin-walled tubes is conducted using the commercial software Hypermesh. Figure 4a presents the isometric view of the FE model, where the mesh size is set to 2×2 mm. All tubes had a uniform length of 250 mm. In crashworthiness studies, since thin-walled tubes cannot be fully compressed, the crushing length is typically set to 70%–80% of the total length[18]. To simplify the numerical procedure and enhance computational stability, a crushing length of 180 mm was adopted.

Figure 4b illustratesthe schematic of the crushing condition. Tubes are usually compressed under quasi-static conditions to evaluate their energy absorption characteristics. In practical quasi-static tests, the loading rate usually ranges from 0.01 to 1 mm/s[19]. To improve the efficiency of the finite element simulation, a rigid plate was applied to compress the tube at a constant velocity of 10 m/s. Given the low mass of the thin-walled tube, its kinetic energy at this speed accounts for only 0.08% of the total absorbed energy, allowing the deformation process to be reasonably approximated as quasi-static. A trigger mechanism is placed 34 mm below the top of the tube, and the bottom of the tube is fully constrained. The total simulation time is set to 0.018 s, and the average computational time for a single simulation was approximately two and a half hours.

The thin-walled tubes in this study are composed of a single material with a Young's modulus of 69 GPa, yield strength of 147.8 MPa, Poisson's ratio of 0.3, and material density of 2580 kg/m^3. The rigid plate is defined using the rigid material model (MAT_20), with an elastic modulus of 210 GPa and a Poisson's ratio of 0.28.



(a) Isometric View of the FE Model (b) Crushing Scenario

Figure 4. FE Schematic Diagram.

The computation and post-processing of the dataset are performed using the commercial software LS-DYNA[20]. Figure 5a shows the simulation result of the thin-walled tube after crushing, with a total crushing displacement of 180 mm. Figure 5b presents the force-displacement curve during the crushing process, where the peak point represents the maximum force. Figure 5c illustrates the mean crushing force at different displacement stages.

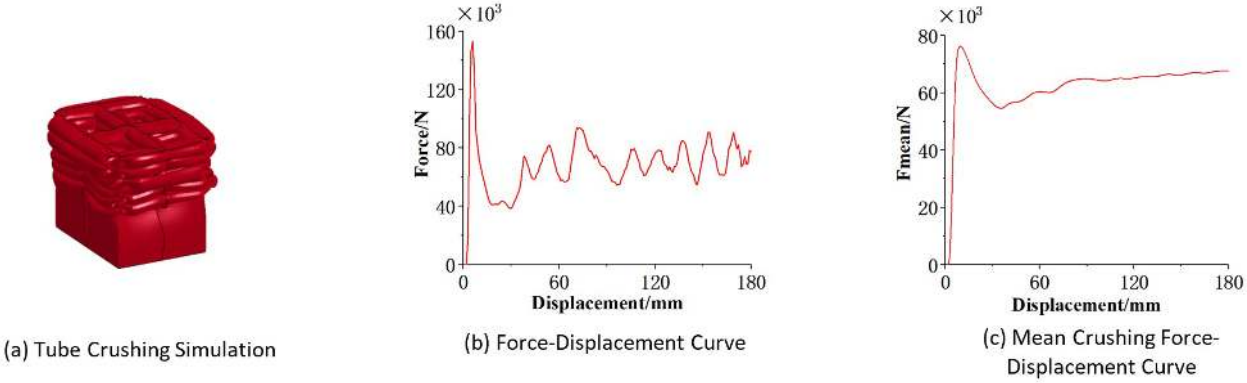

(a) Tube Crushing Simulation (b) Force-Displacement Curve (c) Mean Crushing Force-Displacement Curve

Figure 5. LS-DYNA Simulation Results.

In this study, the peak force and the mean crushing force at a displacement of 180 mm are selected as the prediction targets, while the tube structure serves as the input to build the predictive model.

3.2 Structural Characterization of Multi-Cell Tubes

In this study, the voxelization method[21][22] is employed to digitize the structural information of the FE models of multi-cell tubes. By mapping the FE model into a three-dimensional discrete space based on a Cartesian coordinate system, the structure is represented in a voxelized format. The dimensions of the discrete space are determined by the maximum extents in each coordinate direction to ensure that all sample data are fully encompassed.

For a single sample, let the set of all nodal coordinates be defined as point set *P*. Each voxel in the discrete space is then represented by an index, which is defined as follows:

$$m = (N_x - 1)\left(\frac{P_{(n)x} - P_{x\min}}{P_{x\max} - p_{x\min}}\right), \quad m \in \mathrm{N}+ \tag{2}$$

$$l = (N_y - 1)\left(\frac{P_{(n)y} - P_{y\min}}{P_{y\max} - p_{y\min}}\right), \quad l \in N+ \tag{3}$$

$$n = (N_z - 1)\left(\frac{P_{(n)z} - P_{z\min}}{P_{z\max} - p_{z\min}}\right), \quad n \in N+ \tag{4}$$

where P_{xmin}、P_{ymin}、P_{zmin} and P_{xmax}、P_{ymax}、P_{zmax} represent the minimum and maximum values of the point set *P* in the *x*, *y*, and *z* directions, respectively. Using this indexing method, a voxel occupied by a node is assigned a value of 1, whereas an unoccupied voxel is assigned a value of 0. Through this approach, the geometric characteristics of the multi-cell tubes are systematically defined. As shown in Figure 6, the voxelization process discretizes the geometry into uniform volumetric elements.

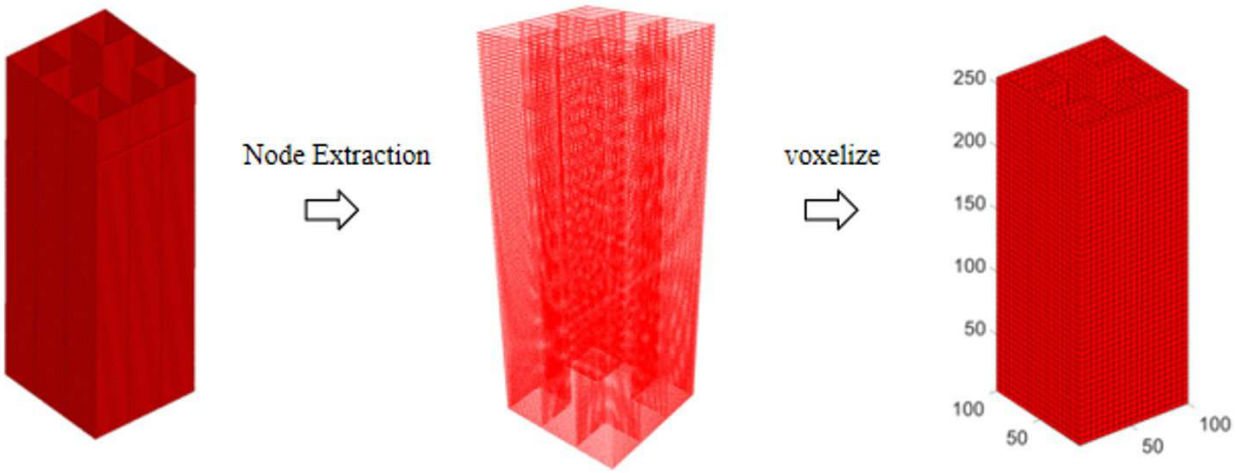

Figure 6. the process of voxelization.

4. MODEL TRAINING AND VALIDATION

4.1 Basic Principles of Autoencoder

To effectively compress the voxelized structure of thin-walled tubes, this study utilizes an autoencoder neural network model for data compression. The autoencoder[23] is an unsupervised learning neural network model that can effectively represent input data, achieving the purposes of data compression and feature extraction.

The autoencoder consists of two parts: an encoder and a decoder. The network architecture is illustrated in Figure 7. The encoder processes input data by encoding it into a latent representation, which captures essential features while reducing dimensionality. The decoder subsequently reconstructs the data from the latent space, ensuring that the extracted representations preserve the critical characteristics of the original input. This enables effective dimensionality reduction while retaining meaningful structural information.

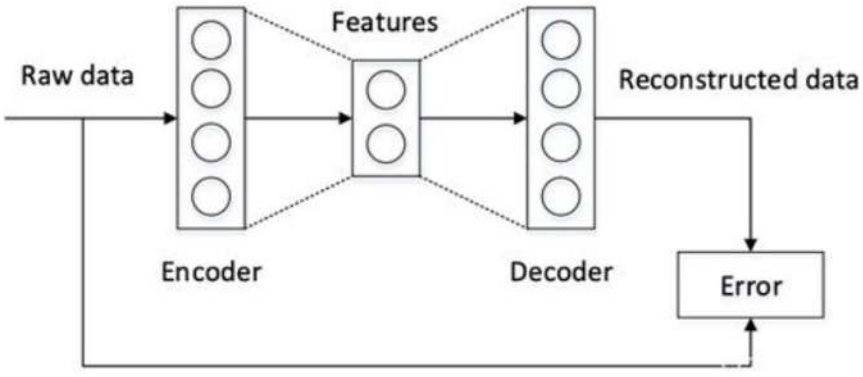

Figure 7. Schematic diagram of the thin-walled tube cross-section.

The crashworthiness prediction process of thin-walled tubes in this paper is constructed as shown in Figure 8. The FE model of the tube is voxelized for structural representation and then used as the input of the autoencoder. In the autoencoder, the structural information of the tube is encoded, transforming the tube's structural information into a one-dimensional latent space. Within the autoencoder, the structural information of the tube is encoded into a one-

dimensional latent space. This space, expressed as a one-dimensional vector, encapsulates the most essential structural features and serves as an efficient surrogate for the full structural representation. It facilitates effective feature extraction and dimensionality reduction. Subsequently, the thickness information and the latent space are combined and input into algorithms such as Support Vector Machines (SVM) or Random Forests to jointly predict the average crushing force and peak force of the tube.

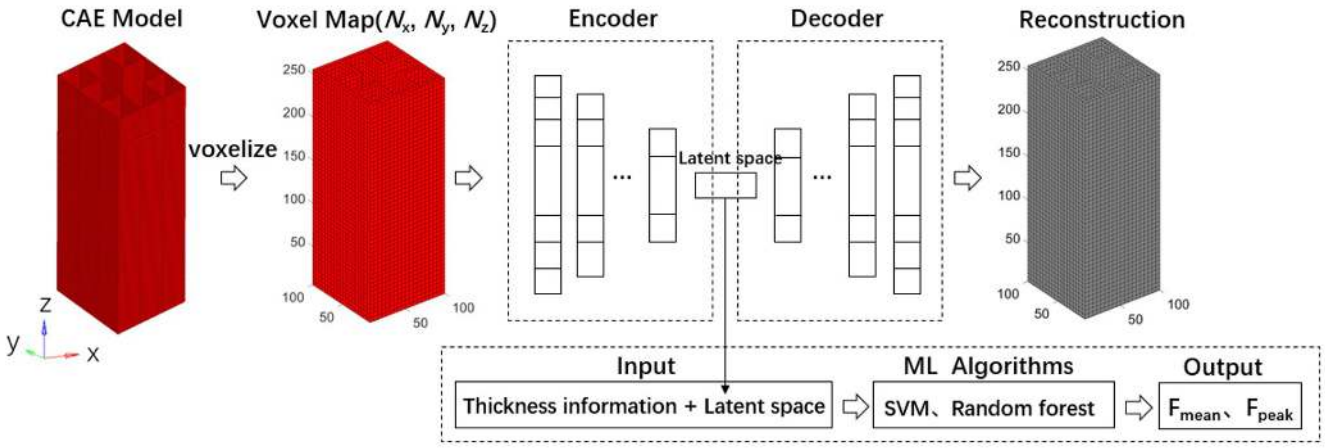

Figure 8. Prediction process diagram.

4.2 Feature Extraction Based on Autoencoder

This study explores different autoencoder architectures, varying latent space dimensions, and voxelization resolutions to establish an optimal feature extraction configuration. As summarized in Table2., four autoencoder variants are constructed based on two voxelization resolutions—(30, 30, 50) and (75, 75, 125)—combined with different encoder–decoder network designs. Here, (N_x, N_y, N_z) denotes the number of divisions along the X, Y, and Z axes, respectively. The lower-resolution voxel grid (e.g., (30, 30, 50)) reduces spatial detail and computational cost, whereas the higher-resolution grid (e.g., (75, 75, 125)) captures finer geometric structures at the expense of increased computational complexity. Each architecture encodes the input into a one-dimensional latent representation of size (1, N_T), where N_T is determined by the voxelization scheme. The most effective configuration is selected based on its empirical performance in downstream tasks.

Table2. Autoencoder Structural Framework.

Voxel Map (Nx, Ny, Nz)	**(30,30,50)**		**(75,75,125)**	
Layer No.	1	2	3	4
1	(1,512)	(1,256)	(1,512)	(1,256)
2	(1,128)	(1,128)	(1,128)	(1,128)
3	(1,16)	(1,16)	(1,16)	(1,16)
4	(1,128)	(1,128)	(1,128)	(1,128)
5	(1,256)	(1,256)	(1,256)	(1,256)
6	(1,512)	(1,1024)	(1,512)	(1,1024)
Output	(1, N_T) --- (N_x, N_y, N_z)			

First, the voxel data of the tube is flattened into one-dimensional information and input into the encoding part of the autoencoder, where the network structure consists entirely of linear layers. The one-dimensional input is progressively mapped to the latent space through the network layers, and subsequently, the decoder reconstructs the original input from the latent space. A loss function is established based on the difference between the output and input. In this process, to ensure that the reconstructed output values fall within the normalized range [0, 1], the Sigmoid activation function is chosen for the output layer; to alleviate the vanishing gradient problem and thus enable faster and

more stable training, the hidden layers utilize the ReLU activation function. The training process employs the Binary Cross Entropy (BCE) function, which is defined as follows:

$$BCE(y,\hat{y}) = -[y \cdot log(\hat{y}) + (1-y) \cdot log(1-\hat{y})] \tag{5}$$

where is the number of samples, represents the actual target values, and represents the model's predicted values. A total of 250 samples are divided into 240 training samples and 10 test samples for evaluating the autoencoder's performance. The batch size during training is set to 16, the learning rate is set to 0.001, and the Adam optimization algorithm is employed[24] . The entire program is implemented in Python using the PyTorch deep learning framework. Model training is performed using an NVIDIA RTX 4090 GPU.

Figure 9 presents the training loss curves for each configuration. Since the initial loss values are relatively high, directly plotting the raw values makes it difficult to compare the training results. Therefore, the loss values are transformed using their natural logarithm, which is used as the vertical axis in the figure. As shown in the figure, the loss values for all four configurations decrease and eventually stabilize with increasing iterations. Among them, Configuration 1 achieves the lowest and most stable training loss. For defining the discrete space, the (30, 30, 50) voxelization setting is sufficient to clearly represent the structural information of the thin-walled tube. Thus, this configuration is selected as the feature extraction scheme.

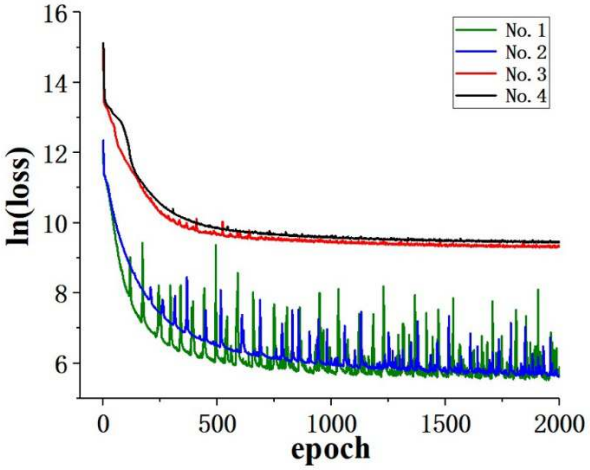

Figure 9. Iterative Loss Curve.

The trained autoencoder model is then evaluated for performance testing. The 10 test samples from the test set are input into the autoencoder to examine the reconstruction quality based on the latent space and evaluate the model's generalization ability. Table 3 presents the detailed mean squared error (MSE) values for the test samples.

Table3. Test Sample Loss Values.

Sample number	MSE value	Sample number	MSE value
1	1.604×10^{-2}	6	2.264×10^{0}
2	4.451×10^{-2}	7	1.344×10^{-3}
3	2.363×10^{-2}	8	1.835×10^{2}
4	1.546×10^{0}	9	1.271×10^{1}
5	4.451×10^{-7}	10	7.921×10^{-2}

To further evaluate the generalization capability of the autoencoder model, this study conducted a detailed comparison between the original structures and the reconstructed structures. Figure 10 presents the comparison results of three original structures and their corresponding reconstructed structures from the test set. As shown in Figure 10, the differences between the reconstructed structures and the original structures are minimal, and their basic feature values (such as length, width, and height) are well preserved. It can also be noted that the reconstruction errors mainly arise from additional structural content in the reconstructed structures, whereas no information is missing in the original

structures. This indicates that the trained autoencoder model has a strong capability to restore structural information, making it a suitable choice for feature extraction.

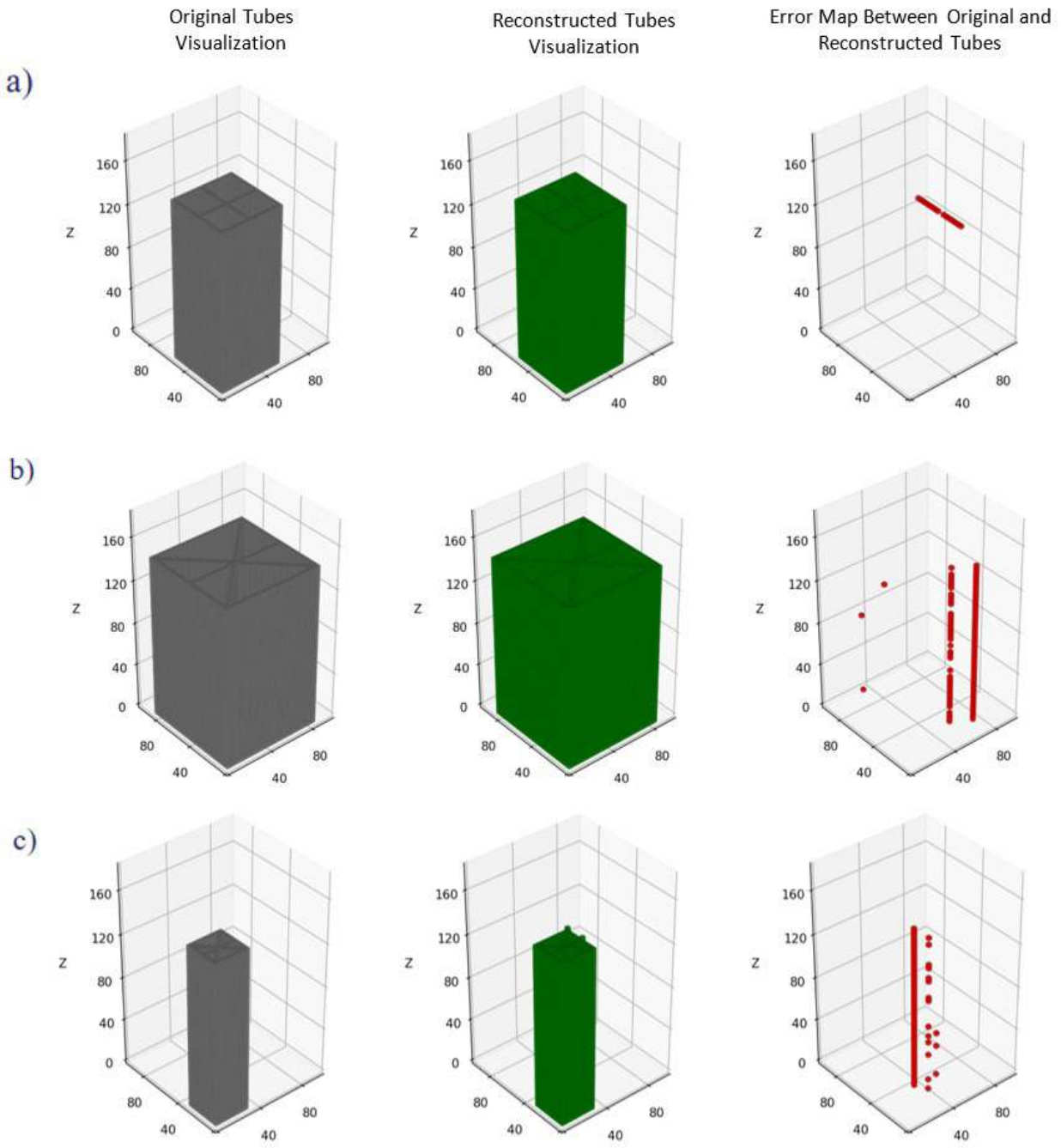

Figure 10. Structural Reconstruction of the Tube.(a), (b), and (c) correspond to different samples selected from the test set.

4.3 Prediction of Crashworthiness of Thin-Walled Tubes

After extracting the structural features, the one-dimensional feature vector from the latent space is used as the structural feature representation. Combined with the thickness information, these features serve as inputs for crashworthiness prediction. Since multiple features are involved, this study evaluates multiple linear regression, support vector machines (SVM), and random forests to identify the most accurate model.

Multilayer Perceptron (MLP)[25] is a type of feedforward neural network widely used for regression and classification as shown in Figure 11. It consists of multiple layers of an input layer, multiple hidden layers, and an output layer, where neurons are fully connected between adjacent layers. The model learns nonlinear relationships by propagating information forward and adjusting weights via backpropagation.

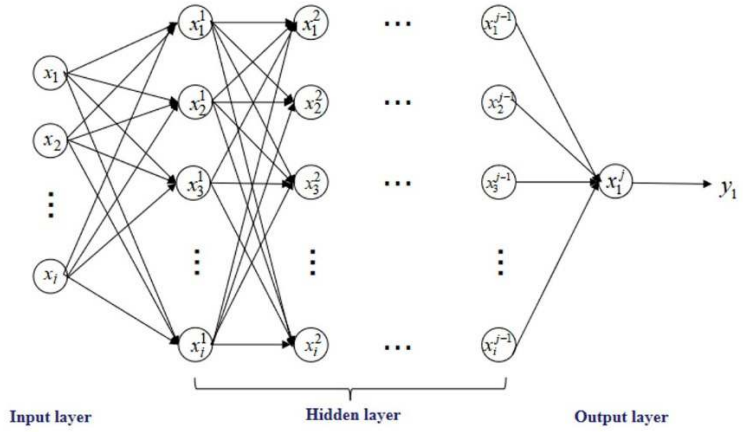

Figure 11. Schematic of the MLP Structure.

Random Forests[26] is an ensemble learning method designed for regression and classification tasks. It consists of multiple decision trees, where each tree is trained on a different random subset of samples and features. By using bootstrap sampling and random feature selection, random forests ensure tree diversity, reduce overfitting risk, and enhance adaptability to various data distributions. Ultimately, the predictions from all trees are aggregated to improve the stability and accuracy of the model.

Support Vector Machines (SVMs) is a supervised learning algorithm, and when applied to regression problems, it is referred to as Support Vector Regression (SVR)[27]. SVR constructs an appropriate regression boundary (regression hyperplane) so that most data points lie within an ε-tube, which is a tolerance margin of width ε around the hyperplane, where points within this region are considered well-fitted. The objective is to maximize the margin between data points outside the ε-tube and the regression hyperplane.

The prediction accuracy for the mean crushing force and peak crushing force is evaluated using the following formula:

$$error = \frac{predicted.value - actual.value}{predicted.value} \times 100\% \tag{6}$$

Table4.presents the test results for predicting mean crushing force using different machine learning models. It can be observed that among the three models, the MLP neural network outperforms the others with the highest accuracy. Therefore, MLP is recommended for predicting mean crushing force.

Table4. Comparison of Machine Learning Models for Mean Crushing Force Prediction

Algorithm	$Error_{max}$	$Error_{min}$	$Error_{mean}$
Random forest Regressor	189.82%	0.66%	24.68%
MLP Neural Networks	52.71%	1.17%	14.21%
Supporting vector Regressor using radial Kernel	147.82%	0.79%	27.72%

Figure 12 shows the prediction performance of the three models on the same test set. It is evident that the MLP neural network not only exhibits lower prediction errors but also maintains better stability in its predictions.

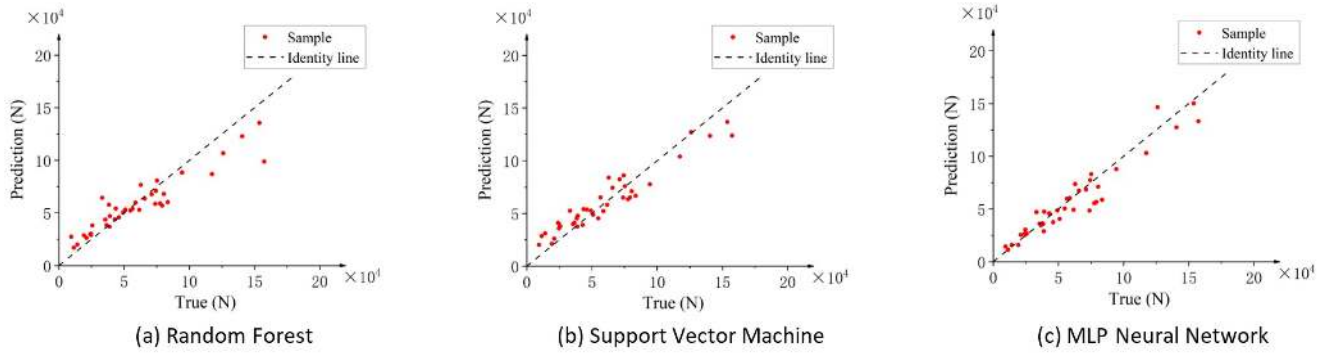

Figure 12. Mean Crushing Force Prediction Results of Three Models.

Table5.compares the machine learning models for peak crushing force prediction. The results indicate that the MLP neural network still achieves the lowest average error, demonstrating its superior predictive performance and better stability compared to the other two models.

Table5. Comparison of Machine Learning Models for Peak Crushing Force Prediction

Algorithm	$Error_{max}$	$Error_{min}$	$Error_{mean}$
Random forest Regressor	158.62%	0.63%	25.22%
MLP Neural Networks	53.43%	0.73%	14.49%
Supporting vector Regressor using radial Kernel	88.11%	0.56%	20.21%

Figure 13 presents the corresponding peak crushing force prediction results for the same test set. It can be seen that the random forest model produces more scattered results, whereas the MLP network exhibits more convergent predictions with better accuracy. Consequently, for predicting both crashworthiness indicators, this study selects the MLP neural network as the final predictive model.

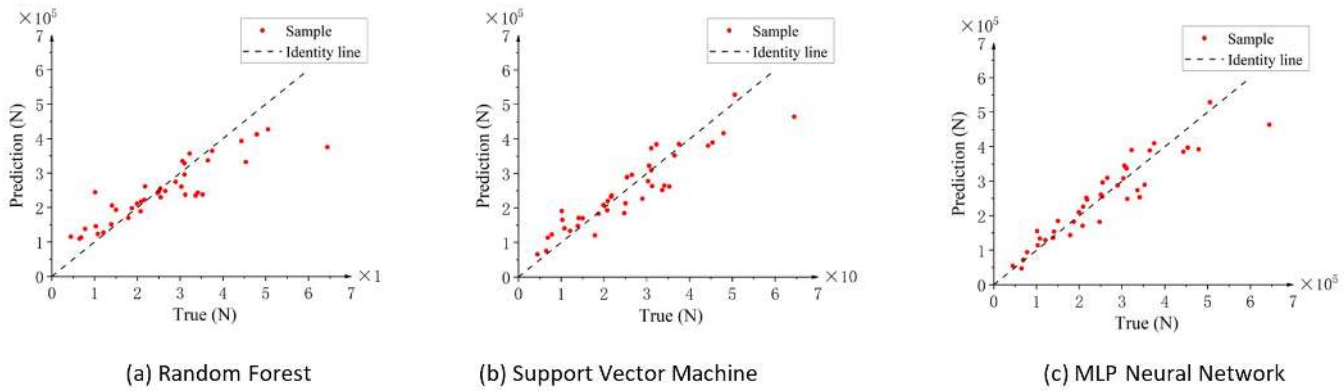

Figure 13. Peak Crushing Force Prediction Results of Three Models.

To further verify the effectiveness of the proposed method, a set of representative thin-walled tube is selected shown in Figure 14 as a case study for the prediction of mean crushing force and peak crushing force.

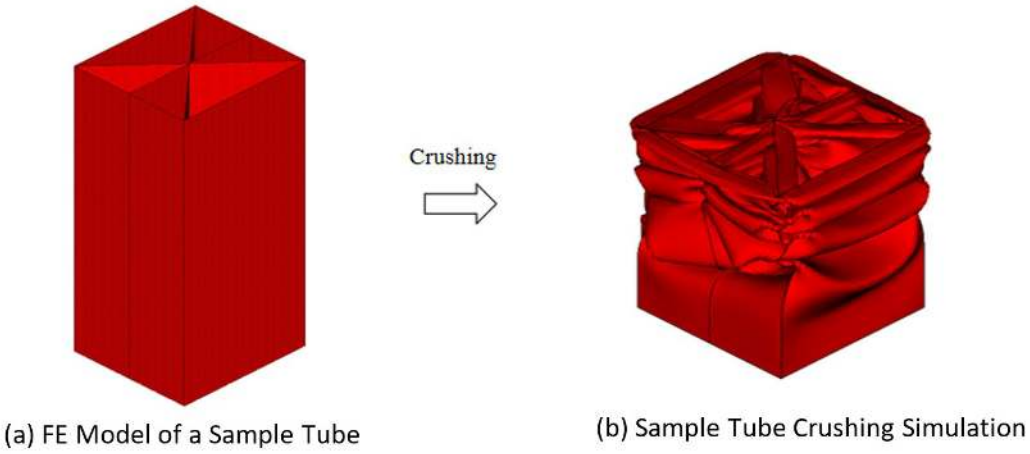

Figure 14. Flowchart of FE Simulation for Thin-Walled Tube Crushing.

First, the voxelized structural data is processed using the previously trained autoencoder model to perform feature compression and extract its latent space representation. The reconstruction results of the autoencoder are shown Figure 15, which demonstrate minimal discrepancy compared to the original data. This indicates that the autoencoder possesses good generalization capability and reconstruction accuracy. Therefore, the one-dimensional latent feature extracted from the autoencoder is adopted for subsequent analysis.

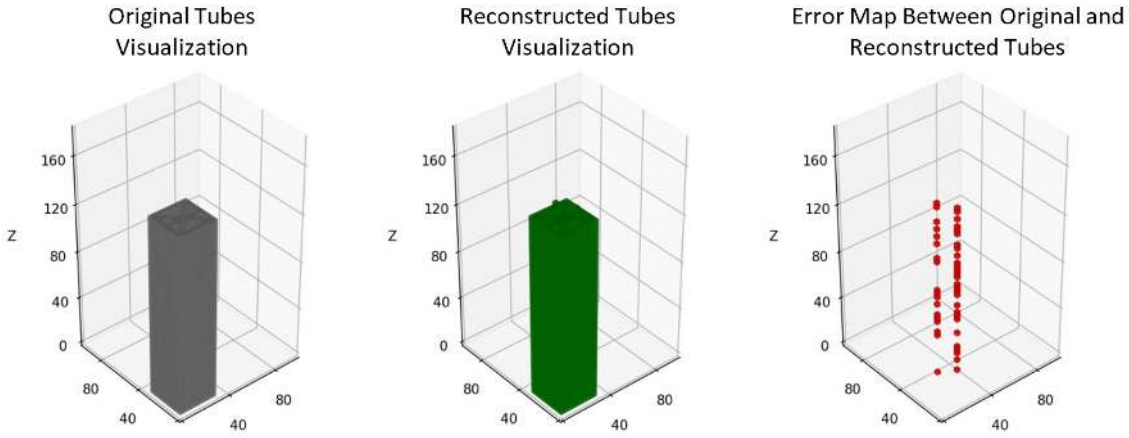

Figure 15. Structural Reconstruction of the Sample Thin-Walled Tube.

Subsequently, the extracted latent features, together with the wall thickness of the thin-walled tube, are used as inputs to the pre-trained Multi-Layer Perceptron (MLP) neural network model, which has demonstrated the best prediction performance. The model is employed to predict the mean crushing force and peak force of the thin-walled tube. The prediction results are shown in the Table6..

Table 6. MLP Neural Network Prediction Results for the Sample Thin-Walled Tube

	CAE Simulation Result (N)	Predicted Value (N)	Error
Mean Crushing Force	106798.7	98577.39	7.70%
Peak Crushing Force	443356	385178.7	13.12%

This workflow is designed to evaluate the generalization ability and prediction accuracy of the combined VAE–MLP model on previously unseen thin-walled tube samples, providing an efficient and feasible approach for the rapid crashworthiness assessment of thin-walled tubes. The prediction for each sample takes only 0.079 seconds, which significantly reduces the computational cost compared to conventional finite element simulations.

5. CONCLUSIONS

This paper proposes a machine learning-based framework for predicting the crashworthiness of thin-walled tubes. The dataset is constructed using FE simulations, where the tube height is standardized, and the cross-sections are parameterized. The Halton sequence sampling method is applied to generate different thin-walled tube models by sampling these parameters. It is important to note that the parameters used for sampling do not participate in the subsequent prediction process; they are solely used for model generation. In total, five different cross-sectional forms of thin-walled tubes are selected to establish 250 simulation samples. After conducting the simulations, the mean crushing force and peak crushing force are extracted as the target variables for prediction.

After obtaining the FE models, the voxelization method is employed to effectively represent the structural characteristics of the tubes while converting them into a data format suitable for machine learning models. Following the proposed framework, the voxelized thin-walled tube models are fed into an autoencoder, which is trained to map the models into a one-dimensional latent space representation that effectively captures their structural features. Additionally, thickness information is incorporated to enhance the representation of the tube models.

Subsequently, three machine learning algorithms—Random Forests, Support Vector Machines (SVM), and Multilayer Perceptron (MLP) neural networks—are evaluated for crashworthiness prediction. The input features consist of the one-dimensional latent space representation generated by the autoencoder along with the thickness information. The dataset is split into 210 samples for training and 40 samples for testing. The results indicate that the MLP neural network achieves the highest prediction accuracy for both mean and peak crushing forces, with the prediction errors of 14.21% and 14.49%, respectively.

In this study, the height of the thin-walled tube models is kept constant. In future work, tube height can be introduced as an additional parameter for training, though this would require a larger dataset to support model training. Moreover, material properties could also be considered. During the voxelization process, structure, material, and thickness information can be represented using three separate channels to comprehensively describe the tube characteristics. Additionally, a 3D convolutional autoencoder could be explored for feature extraction of the tube structures.

In summary, this study establishes a machine learning-based framework for predicting the crashworthiness of thin-walled tubes. By predicting mean and peak crushing forces under impact conditions, the proposed framework significantly reduces simulation costs and offers an alternative approach for evaluating thin-walled tube performance.

Author's Contributions: Investigation, Hongbin Tang, Ledan Liu; Methodology, Hongbin Tang, Ledan Liu; Conceptualization, Hongbin Tang, Zheng Dou; Writing - Reviewing & Editing, Ledan Liu, Zheng Dou, Zihang Li; Writing Original draft, Hongbin Tang, Zheng Dou, Zihang Li.

Data availability: No data was used for the research described in the article.

Editor: Marcílio Alves

REFERENCES

[1]. W. Hou, P. He, Y. Yang, et al., Crashworthiness optimization of crash box with 3Dprinted lattice structures, Int. J. Mech. Sci. 247 (2023), 108198.

[2]. Xiao Y, Long H, Lu S, et al. Optimization of crashworthiness of CFRP thin-walled beams filled with aluminium honeycomb based on surrogate model[J]. International Journal of Crashworthiness, 2023: 1-10.

[3]. X. Zhang, H. Zhang, W. Ren, Bending collapse of folded tubes, Int. J. Mech. Sci. 117 (2016) 67–78.

[4]. Z. Liu, J. Liu, J. Liu, et al., The impact responses and failure mechanism of composite gradient reentrant honeycomb structure, Thin-Walled Struct. 182 (2023), 110228.

[5]. Ruyang Yao,Tong Pang,Bei Zhang,et al. On the crashworthiness of thin-walled multi-cell structures and materials: State of the art and prospects[J]. Thin-Walled Structures,2023,Vol.189: 110734.

[6]. Zheng G, Pang T, Sun G, et al. Theoretical, numerical, and experimental study on laterally variable thickness (LVT) multi-cell tubes for crashworthiness[J]. International Journal of Mechanical Sciences, 2016, 118: 283-297.

[7]. Lu B, Zhang J, Zheng D, et al. Theoretical analysis on CFRP/Al hybrid multi-cell tubes under axial crushing loading[J]. European Journal of Mechanics-A/Solids, 2023, 97: 104815.

[8]. Lu B, Shen C, Zhang J, et al. Study on energy absorption performance of variable thickness CFRP/aluminum hybrid square tubes under axial loading[J]. Composite Structures, 2021, 276: 114469.

[9]. Jeon J, Kim J, Lee J J, et al. Development of deep learning-based joint elements for thin-walled beam structures[J]. Computers & Structures, 2022, 260: 106714.

[10]. Ghasemi M, Silani M, Yaghoubi V, et al. Performance Prediction of Thin-Walled Tube Energy Absorbers Using Machine Learning[C]//International Symposium on Industrial Engineering and Automation. Cham: Springer International Publishing, 2022: 87-99.

[11]. Kohar C P, Greve L, Eller T K, et al. A machine learning framework for accelerating the design process using CAE simulations: An application to finite element analysis in structural crashworthiness[J]. Computer Methods in Applied Mechanics and Engineering, 2021, 385: 114008.

[12]. Weigang Chen,Tomasz Wierzbicki. Relative merits of single-cell, multi-cell and foam-filled thin-walled structures in energy absorption[J]. Thin-Walled Structures,2001, Vol.39(4): 287-306.

[13]. Zhang, X (Zhang, Xiong),et al. Theoretical prediction and numerical simulation of multi-cell square thin-walled structures[J]. Thin-Walled Structures,2006, Vol.44(11): 1185-1191.

[14]. Jian Xie, Junyuan Zhang,Zheng Dou,et al. An explainable machine learning method for predicting and designing crashworthiness of multi-cell tubes under oblique load[J]. Engineering Applications of Artificial Intelligence,2025,Vol.147: 110396.

[15]. Bigdeli A, Damghani Nouri M. Investigation of the numerical, experimental, statistical and optimization of thin-walled energy absorber with novel configuration using response surface method under axial loading. Journal of Sandwich Structures & Materials. 2018;22(8):2735-2767.

[16]. Anderson M J, Whitcomb P J. DOE simplified: practical tools for effective experimentation[M]. CRC press, 2017.

[17]. Yao S, Yan K, Lu S, et al. Prediction and application of energy absorption characteristics of thin-walled circular tubes based on dimensional analysis[J]. Thin-Walled Structures, 2018, 130: 505-519.

[18]. Yao Yu,Xiaobo Gong,Jialin Li,et al. Crashworthiness performance and optimization of multi-cell aluminum tubes under axial loading[J]. Structures,2023,Vol.55: 1556-1571.

[19]. A.G. Hanssen,M. Langseth,O.S. Hopperstad. Static and dynamic crushing of square aluminium extrusions with aluminium foam filler[J]. International Journal of Impact Engineering,2000,Vol.24(4): 347-383.

[20].Hallquist J O. LS-DYNA theory manual[J]. Livermore software Technology corporation, 2006, 3: 25-31.

[21]. Karabassi E A, Papaioannou G, Theoharis T. A fast depth-buffer-based voxelization algorithm[J]. Journal of graphics tools, 1999, 4(4): 5-10.

[22]. Hinks T, Carr H, Truong-Hong L, et al. Point cloud data conversion into solid models via point-based voxelization[J]. Journal of Surveying Engineering, 2013, 139(2): 72-83.

[23]. Meng Q, Catchpoole D, Skillicom D, et al. Relational autoencoder for feature extraction[C]//2017 International joint conference on neural networks (IJCNN). IEEE, 2017: 364-371.

[24]. Kingma D, Ba J. Adam: A method for stochastic optimization. 2014.

[25]. Jia Li,Rongchao Yang,Xinyan Cao, et al. Inception MLP: A vision MLP backbone for multi-scale feature extraction[J]. Information Sciences, 2025, Vol.701: 121865.

[26]. Breiman L. Random forests[J]. Machine learning, 2001, 45: 5-32.

[27]. Smola A J, Schölkopf B. A tutorial on support vector regression[J]. Statistics and computing, 2004, 14: 199-222.